ELSEVIER

Journal of Physics and Chemistry of Solids 65 (2004) 639–645

JOURNAL OF PHYSICS AND CHEMISTRY OF SOLIDS

www.elsevier.com/locate/jpcs

Carbothermally-assisted aerosol synthesis of semiconducting materials in the system GaN/Mn

Jerzy F. Janik[a,*], Mariusz Drygaś[a], Cezary Czosnek[a], Maria Kamińska[b], Maria Palczewska[c], Robert T. Paine[d]

[a]*AGH University of Science and Technology, Faculty of Fuels and Energy, al. Mickiewicza 30, 30-059 Kraków, Poland*
[b] *Warsaw University Institute of Experimental Physics, ul. Hoża 69, 00-681 Warsaw, Poland*
[c]*Institute of Electronic Materials Technology, ul. Wólczyńska 133, 01-919 Warsaw, Poland*
[d]*University of New Mexico, Department of Chemistry, Albuquerque, NM 87131, USA*

Abstract

Aerosol-assisted vapor phase synthesis aimed at preparation of magnetic semiconductor nanopowders of $Ga_{1-x}Mn_xN$ is carried out both from aqueous and methanol solution mixtures of gallium nitrate and manganese (II) nitrate. After an additional pyrolysis at 1000 °C under an ammonia flow, the light colored products are characterized with XRD, SEM/EDX, EPR, BET surface area determinations, helium pycnometry, and oxygen analyses. The characterization data for the powders are consistent with the formation of composites of nanosized manganese-doped hexagonal GaN and regular MnO phases.

1. Introduction

Nanosized Group III-nitrides are often preferred for advanced electronic applications that implement breakthrough technologies [1–3]. 'Blue' emitters, luminescence devices, spintronics, and photonic crystals represent a few prominent examples of either emerging or potential utilizations for the heavy Group III materials. Isoelectronic with graphite and, at the same time, more oxidation resistant boron nitride powders offer other advantageous properties including in thermal management composites and adsorbents for specific gas separations [4].

While there are continued efforts in search of new precursor routes to simple III–Vs, there appears to be a significant trend toward development of synthesis and processing of more complex systems. For example, boron nitride BN doped with rare-earth metals is reported to combine its advantageous thermal properties with the luminescence features of the rare-earth metal centers [5] while BN nanoparticles encapsulated in zeolite are found to emit in the blue region of UV–vis [6]. Similarly, rare-earth doped GaN is considered for applications in emitters/optical communication systems [7] and in full color light sources [8].

The coexistence of ferromagnetism and semiconducting properties in one material (magnetic semiconductors) offers an attractive area for combining the advantages of both in spintronics [2,9,10]. In this regard, the GaN/Mn system has recently become the subject of extensive research especially after it was predicted that GaN-based diluted magnetic semiconductors might have Curie temperatures exceeding room temperature [10,11].

One of the approaches to study such phenomena is to dwell on thin Mn-doped GaN films [10a,b]. One can also incorporate Mn-centers into bulk microcrystalline GaN as was successfully done by some of the co-authors of this report [11]. In this case, the synthesis of the polycrystalline material was accomplished by the so-called AMMono method [11d]. In the particular case of the $Ga_{1-x}Mn_xN$ preparation, the as-prepared GaN powders were mixed with powdered manganese metal and the mixture was heated at 1230–1250 °C under an ammonia flow for several hours. The GaN-doped large single crystals grew directly on the GaN powder bed and up to 2 wt% of manganese could be incorporated in such crystals [11c].

Herein, we describe attempts to utilize the aerosol-assisted vapor phase synthesis (AAVS) methodology to

* Corresponding author.
E-mail address: janikj@uci.agh.edu.pl (J.F. Janik).

0022-3697/$ - see front matter © 2003 Elsevier Ltd. All rights reserved.
doi:10.1016/j.jpcs.2003.10.044

prepare Mn-doped GaN powders based on modifications of this simple and versatile method already successfully applied to make BN [12a] and GaN [12b] powders. The AAVS method was easily adapted to make Mn-doped GaN and/or composite GaN/Mn-based materials by use of aqueous solutions containing both gallium nitrate and manganese (II) nitrate. Also, the aerosol synthesis was explored by using methanol solutions of the salts. The carbothermally-assisted reduction chemistry in such systems was expected to preferentially drive the nitridation reactions toward low oxygen products. The combination of advantages of the aerosol method with its nanosized region of particle evolution was expected to offer some potential for making manganese-doped gallium nitride powders.

2. Experimental

2.1. Aqueous solutions

$Ga(NO_3)_3{\cdot}x\,H_2O$ and $Mn(NO_3)_2{\cdot}x\,H_2O$ ($x = 4–6$) (Aldrich) were used to make both aqueous and methanol solutions. For gallium nitrate, x was assumed at 9 [13c] while for manganese nitrate at 4 to prepare solutions with three Ga/Mn atomic ratios labeled 20/1(H_2O) for Ga:Mn = approx. 20:1, 10/1(H_2O) for Ga:Mn = approx. 10:1, and 5/1(H_2O) for Ga:Mn = approx. 5:1. For example, for the 20/1(H_2O) solution, 25.00 g (0.05985 mol) of gallium nitrate and 0.82 g (0.00305) mol of manganese (II) nitrate, Ga:Mn = approx. 19.6, were dissolved in 460 ml of deionized water affording around 480 ml of a solution, about 0.12 M in Ga^{+3} ions. The solutions were used in aerosol generation experiments to afford raw powders at 1050 °C, NH_3 flow = 3.0 l/min, N_2-carrier flow = 1.0 l/min [12b]. Typically, a batch of 480 ml of a solution after a 12–15 h run afforded around 2 g of a raw powder. For reference purposes, 200 ml of the manganese (II) nitrate solution (30.00 g in 300 ml H_2O) were used in a 5 h aerosol generation yielding 1.5 g of a dark green powder. Similarly, a powder was made from the pure gallium nitrate solution [12b]. The raw powders were then pyrolyzed at 1000 °C for 5 h with an NH_3 flow of 0.2 l/min. All products were characterized by XRD (Siemens D5000 diffractometer, Cu Kα source), SEM/EDX (Hitachi S-800), EPR (Bruker ESP-300 X-band spectrometer), and oxygen analysis (Saint-Gobain Adv. Ceram. Corp., Amherst, NY, USA) while helium density (Micromeritics AccuPyc) and BET surface area (Micromeritics Gemini 2360) were determined for selected samples. The analytical results included for (i) *reference manganese product (MnO)*: mass loss during pyrolysis, 7%; O, 22.8%; BET, 1.1 m^2/g; d_{He}, 6.0 g/cm^3, for (ii) *reference GaN*: mass loss during pyrolysis, 9%; O, 1.6%, for (iii) 20/1(H_2O): mass loss during pyrolysis, 5%; O, 1.8%; d_{He}, 6.0 g/cm^3, for (iv) 10/1(H_2O): mass loss during pyrolysis, 8%; O, 3.0%; BET, 0.5 m^2/g, d_{He}, 6.1 g/cm^3, and for (v) 5/1(H_2O): mass loss during pyrolysis, 12%; O, 4.4%.

2.2. Methanol solutions

Both $Ga(NO_3)_3{\cdot}x\,H_2O$ and $Mn(NO_3)_2{\cdot}x\,H_2O$ are soluble in methanol. The methanol solutions were labeled as 20/1(MeOH) for Ga:Mn = approx. 20:1 and 10/1(MeOH) for Ga:Mn = approx. 10:1. The 5/1(MeOH) ratio was not investigated. For reference purposes, 25.00 g of $Ga(NO_3)_3{\cdot}x\,H_2O$ were dissolved in 460 ml of methanol and the solution was used in a 7 h run affording 1.4 g of a black product. Similarly, a reference raw powder was made from the solution of 25.00 g of $Mn(NO_3)_2{\cdot}x\,H_2O$ in 460 ml MeOH, 7 h run, 2.9 g yield of powder (no soot formation observed). Relatively lower yields from the methanol solutions were obtained that were caused by a tendency of the sooty powders to stick to the sides of the tube due to unfavorable experimental design of the set-up specifically built for aqueous solution process characteristics. This phenomenon could be minimized by suitable design/experimental changes. All the raw powders were subsequently pyrolyzed at 1000 °C for 5 h with an NH_3 flow of 0.2 l/min yielding similar products as observed in the aqueous systems. The analytical results included for (i) *reference manganese product (MnO)*: mass loss during pyrolysis, 3%; O, 21.3%; d_{He}, 5.7 g/cm^3, for (ii) *reference GaN*: mass loss during pyrolysis, 10%; O, 1.0%, for (iii) 20/1(MeOH): mass loss during pyrolysis, 10%; O, 0.9%, and for (iv) 10/1(MeOH): mass loss during pyrolysis, 21%; O, 1.9%.

3. Results and discussion

We successfully applied the convenient AAVS method to make a range of GaN-based composites containing manganese. Our approach included the use of traditional aqueous solutions (confirmed to make spheroidal powders of BN and GaN [12]) as well as a new attractive method modification that used methanol solutions of $Ga(NO_3)_3{\cdot}x\,H_2O$ and $Mn(NO_3)_2{\cdot}x\,H_2O$. In general, the method enables combining the soluble substrates in the solution that is then used to generate aerosol powders and, potentially, creating advantageous conditions for forming composite products mixed on the molecular level. Under such circumstances, one can envision the formation of a range of otherwise difficult to make solid state products including kinetically controlled metastable phases, solid solutions, and nanocrystalline assemblages. The first synthesis step, done under an ammonia rich atmosphere, results in thermal cracking and partial nitridation chemistry of the precursor. In the second step, the raw powder is subjected to pyrolysis, *i.e.*, at 1000 °C for the gallium system, under an ammonia flow intended to complete the nitidation reactions. Also, our previous experience with using methanol solvent in some precursor systems for BN powders convinced us that its presence could help in achieving raw powders with less oxygen than found in those from aqueous solutions supporting the cooperating

carbothermal reduction chemistry taking place under experimental conditions of the AAVS method [13].

3.1. Aqueous solutions

All of the composite systems yield light colored powders with oxygen contents ranging from 1.8% for 20/1(H_2O) to 4.4% for 5/1(H_2O) while for the reference pure gallium and pure manganese products the values are 1.6% and 22.8%, respectively. Based on the expected formation of GaN, these O-content levels suggest that the manganese component does not undergo significant nitridation, if at all. Actually, the theoretical oxygen content in MnO is 22.6%, which can be compared with the 22.8% value found above. On the other hand, the observed value of 1.6% for the reference GaN product appears to be in the upper range of residual O-contents for GaN powders prepared previously from aqueous solutions.

The XRD patterns for all three composite powders and two pure phases clearly indicate that the former ones are composed mostly of the respective hexagonal GaN (h-GaN) and cubic MnO lattices (Fig. 1). Additionally, a detailed examination of the patterns for the 10/1(H_2O) and 20/1 (H_2O) powders indicates a presence of minute quantities of Mn_3N_2 and Mn_4N, respectively. The X-ray data are consistent with the O-analyses. Apparently, the bulk of the manganese precursor is not nitrided but undergoes simple thermal decomposition. The average crystallite diameters (Scherrer's equation, $K = 1$) are for the pure MnO product in the 90–100 nm range and for the 10/1(H_2O) composite: h-GaN, 70–80 nm and MnO, 35–40 nm.

In this regard, there seems to be no *a priori* structural basis to expect the formation of stable solid solutions of manganese nitride phase(s) in the h-GaN structure or *vice versa*. The known polytypes of manganese nitride encompass θ (MnN), η (Mn_3N_2), ζ (Mn_5N_2, Mn_2N, and $MnN_{0.86}$), and ε(Mn_4N) phases [14]. The θ, η, and ε phases are reported to have (fct) or (fcc) cubic structures and ζ is described as the *anti* α-PbO_2 type while it is suggested that ordered or random N-vacancies may be quite common in the Mn–N system. Similarly, there is a large mismatch between the cell parameters of the zinc blende c-GaN and of the Mn-nitride polytypes. However, the aforementioned tendency of the manganese nitrides to form N-vacancy defected structures may offer some potential of incorporating Mn-centers into gallium nitride as reported for microcrystalline h-(Ga, Mn)N powders [11] and calculated for c-GaN [10e]. In the related area, intentionally Mg- and Si-doped h-GaN lattices are well established [15]. Concerning the XRD results above and in light of the expected limited solubility of manganese in h-GaN, one can conclude that the XRD data while indicating the major types of lattices, *i.e.*, h-GaN and cubic MnO, do not discriminate against the possibility of the host phase being doped by a guest metal center.

Fig. 2 presents the SEM images of the pure GaN and MnO products. The GaN sample (Fig. 2A) consists of rather large particles, many of them showing spheroidal morphology. This suggests that an individual microsized particle, which is likely derived from an aerosol generated parent sphere, may be composed of a number of nanocrystallites of GaN (see, XRD results above). For MnO (Fig. 2B), there appears to be a growth of sharp-edged crystallites resulting in macroscopic sintering of the product.

In Fig. 3, the SEM images of the composites are shown. As it is seen for 5/1(H_2O) (Fig. 3A), the powder's overall morphology is more reminescent of the related pure GaN powder (Fig. 2A) than of the pure MnO (Fig. 2B). A similar picture emerges from the 10/1(H_2O) system (Fig. 3B). It is likely that the coexistence of the two components in this composition range imposes definite constraints on crystal growth of the two separate phases. Accordingly, the average MnO crystallite sizes in the composite systems are significantly smaller, 2–3 times, than in the pure MnO. For 20/1(H_2O) (Fig. 3C), a characteristic feature is the presence of abundant rod-like crystallites and much smaller whiskers. These morphologies are confirmed by EDX measurements to be mostly if not exclusively GaN.

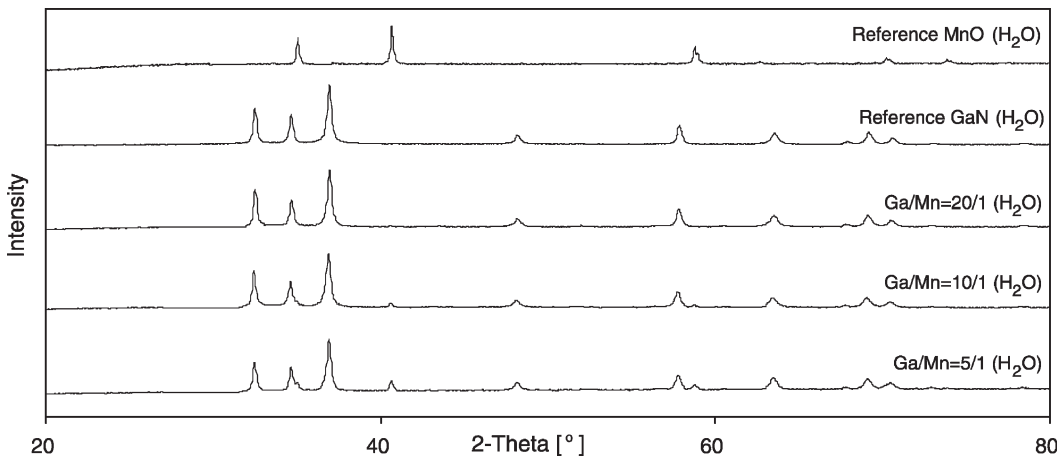

Fig. 1. XRD patterns for composite and reference powders obtained via aqueous solutions.

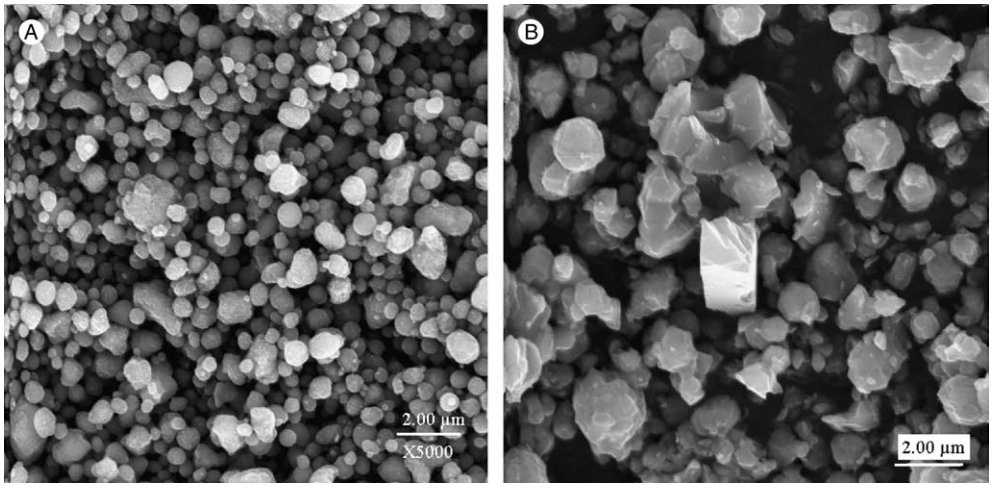

Fig. 2. SEM micrographs of reference powders: A—GaN(H_2O); B—MnO(H_2O).

Apparently, in this system with the smallest amount of Mn, the co-crystallization is dominated by the growth of bulk h-GaN although other crystal growth phenomena may manifest themselves as well. These could include a known catalytic mechanism involving transition metal promoted whisker/rod growth or similar gas phase reactions [16].

The EDX analysis of all of the composites clearly indicates nonuniform manganese distribution suggesting that the materials are compositionally heterogeneous. In this regard, there are regions noticeably enriched in manganese or gallium with respect to the average composition signal ratio. Due to the accuracy limitations of our EDX measurements, we cannot strictly prove the existence of the suggested pure phases by the XRD data, i.e. h-GaN and MgO, in the composites. However, the results support their existence while not excluding the host phase doped with the guest metal center even up to a few atomic percents.

The EPR measurements (X-band, 9.4 GHz) yield for each composite a single structureless resonance signal of *g*-factor equal to 2.008 ± 0.003 (Fig. 4). The *g*-value of 2.005 ± 0.003 for the reference GaN sample with apparent nonintentional Mn contamination (Fig. 4B, a), differs slightly from the above results which, most likely, can be attributed to the less accurate determination associated with the 'wave' curvature of the line. The Mn^{+2} defects ($3d^5$, $S = 5/2, I = 5/2$) were initially observed by EPR in thin layers of Mn-doped GaN deposited on sapphire [17]. Therein, the line of $g = 1.999$ showed a fine splitting into five components, each with a six-fold hyperfine splitting due to the interaction of an electron spin with a Mn-nuclear spin. On the other hand, for the microcrystalline Mn-doped GaN powders obtained by the AMMono method, the $+1/2 \rightarrow -1/2$ transition with a six-fold splitting was only observed for low Mn-concentrations while for higher concentrations only one broad line with hyperfine splitting more or less marked and with $g = 2.000 \pm 0.003$ was seen [11a,b]. In this regard, the presence of a single broad line was typically claimed in different semiconductors highly doped with Mn and ascribing to Mn^{+2} pairs or bigger clusters of interacting Mn^{+2} ions [18]. It is also known that exchange interactions lead to narrowing of EPR lines. Therefore, the observed structureless lines are strong indication of high concentration of Mn^{+2} ions and exchange interactions among them. A slightly higher *g*-factor for the interacting *vs.* isolated Mn^{+2} ions was reported in the related system ZnS/Mn [18].

Fig. 4A shows a composite picture of all normalized resonances (re-scaled to the same amplification factor and sample volume) while Fig. 4B presents only the as-obtained resonances. Since all the linewidths are comparable

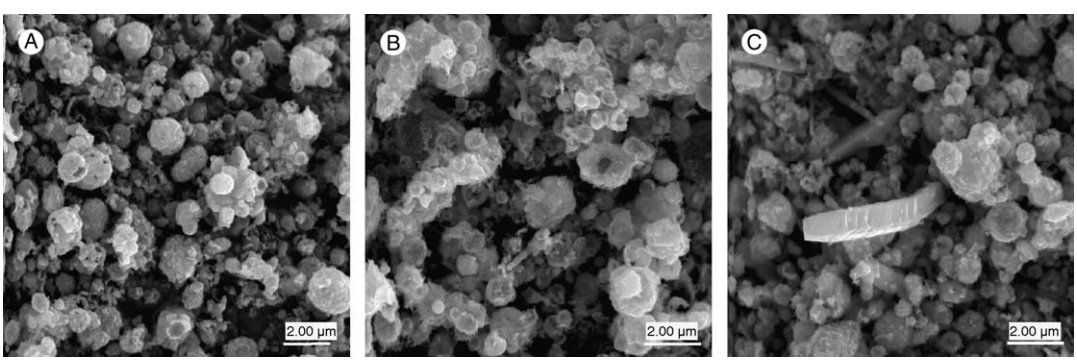

Fig. 3. SEM micrographs of composites from the aqueous solution systems: A—5/1(H_2O); B—10/1(H_2O); C—20/1(H_2O).

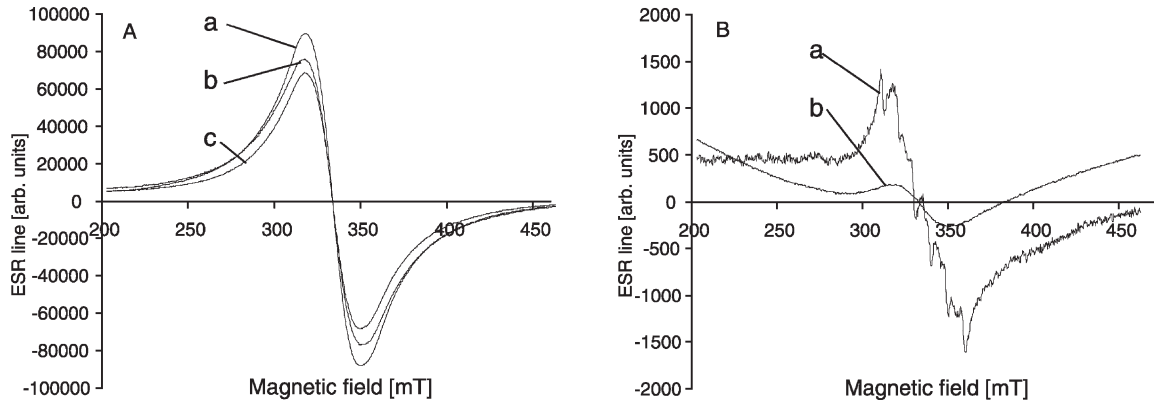

Fig. 4. Normalized EPR resonance lines for composite (A) and reference (B) powders obtained *via* aqueous solutions; A: a—5/1(H_2O), b—10/1(H_2O), c—20/1(H_2O); B: a—reference GaN, b—reference MnO.

(approx. 32 mT), differences in the line magnitudes correspond to differences in the concentrations of paramagnetic defects. It can be seen (Fig. 4A) that the concentration of paramagnetic defects slightly increases with the relative amount of manganese in the system; however, the dependence is not proportional but it rather bears features of a saturation effect. In conclusion, it is apparent that the *g*-values obtained in this study for the nanosized powders *via* the AAVS aqueous route are larger than those for single crystals and microcrystalline powders of manganese doped GaN. With respect to the make-up of the AAVS composite powders, the EPR results seem to be consistent with the existence of specific paramagnetic defects associated with Mn(d^5) centers.

3.2. Methanol solutions

The O-contents are for 10/1(MeOH) and 20/1(MeOH), 1.9% and 0.9%, respectively, and for the reference GaN (MeOH) and manganese product, 1.0% and 23.2%, respectively. The latter values suggest that, first, the pure GaN powder contains less oxygen than the GaN powder from the aqueous solution system and, second, the major manganese product is again MnO. Apparently, the carbothermal reduction chemistry results in lower residual oxygen contents in GaN but it has no influence on promoting nitridation in the manganese systems.

The XRD patterns for the composites here are very similar to those shown in Fig. 1 and they confirm the presence of the prevailing h-GaN with the minor cubic MnO. On the one hand, it is encouraging that the AAVS method can successfully be extended to the methanol solutions to make low oxygen GaN powders. On the other hand, it is a bit disappointing that the use of methanol has no impact on MnO nitriding. Again, the XRD results do not preclude the possibility that the h-GaN phase in the composites could be doped with Mn-centers.

There appears to be a striking difference in morphology between the pure GaN powders obtained *via* the aqueous (Fig. 2A) and the methanol (Fig. 5A) routes. In the former case, spheroidal particles are mostly seen while, in the latter case, the well shaped large crystallites are embedded in the matrix of abundant much smaller fine particles. Rarely visible are particles in between the two extremes. On

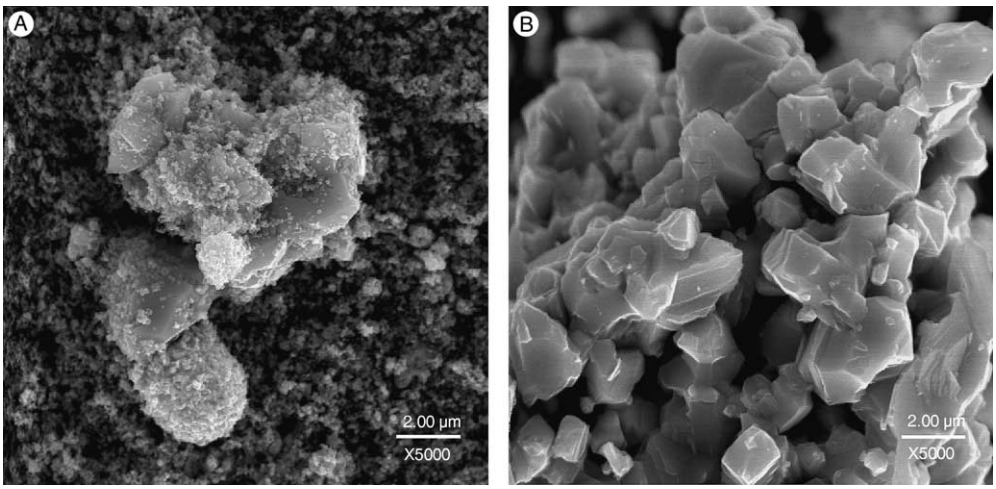

Fig. 5. SEM micrographs of reference powders: A—GaN(MeOH); B—MnO(MeOH).

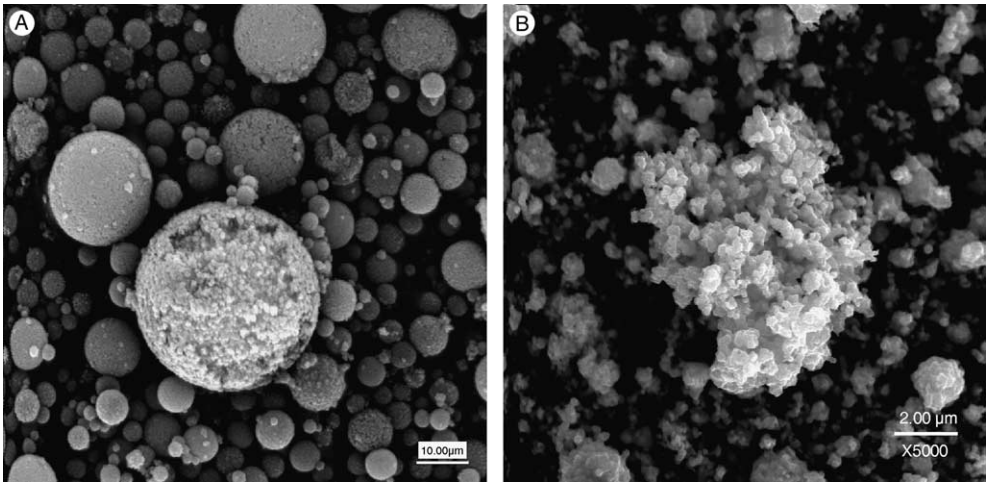

Fig. 6. SEM micrographs of composites from the methanol solution systems: A—10/1(MeOH); B—20/1(MeOH).

the other hand, the appearance of MnO (Fig. 5B) is similar to its 'aqueous' counterpart showing, again, a heavily sintered product.

The SEM images for the composites obtained via methanol route, 10/1(MeOH) and 20/1(MeOH), are presented in Fig. 6 in, A and B, respectively. For 10/1(MeOH), the characteristic and striking feature is a regular spherical morphology. Many of the large spheres appear to be rather soft and the fractured areas/cracked surfaces expose fine crystallites inside them. The morphologies of the two powders are somewhat similar to each other but differ significantly from the comparable cases in the aqueous systems. For example, there are no rod-like/whisker features in the 20/1(MeOH) product that are so typical for the relevant 20/1(H_2O) product. This indicates basically different nitridation/cracking reaction mechanisms operating in these solvent environments.

The EDX examination of both composites supports their compositional heterogeneity. It appears, however, that the observed Ga/Mn distributions are not reflected by any specific microstructural features. Also, the results confirm the fact that even the assisted carbothermal reduction chemistry does not enable the nitridation of the manganese precursor. It is instructive to note that the prevailing crystallization of the stable MnO is seen in all cases.

Fig. 7 represents the EPR data obtained for the materials *via* methanol route. As was the case of the relevant aqueous solution systems, the higher manganese content in the composites is reflected by the higher signal intensity of the broad structureless resonance line, $g = 2.008 \pm 0.003$, not proportionally, though (Fig. 7A). These values are comparable with the quantities in the aqueous system and support a similar nature of the paramagnetic defects in both cases. In this regard, it is interesting to note that the intensities of the resonance lines for the materials derived from the methanol system are about twice as large as the intensities for those from the aqueous system. This indicates significantly larger amounts of paramagnetic defects in the powders derived *via* the methanol route. This may suggest that better conditions for manganese incorporation into the GaN matrix exist in the methanol solution system both in terms of the structural and/or surface aspects.

With the similar nature of the paramagnetic defects in all of the investigated materials demonstrated by the broad, structureless resonance lines, $g = 2.008$, their structural basis and linkage to potential Mn^{+2}/GaN centers remain at

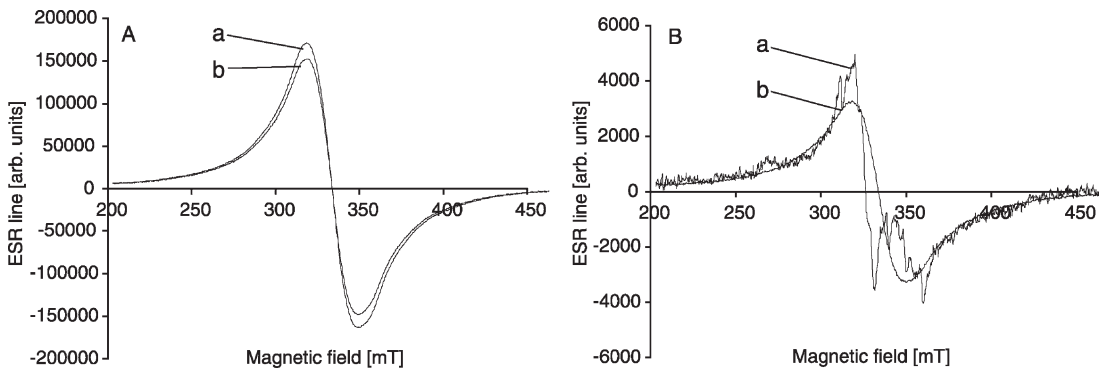

Fig. 7. Normalized EPR resonance lines for composite (A) and reference (B) powders obtained *via* methanol solutions; A: a—10/1(MeOH), b—20/1(MeOH); B: a—reference GaN, b—reference MnO.

this point unclear. Certainly, the new nanocrystalline size regime of the currently studied Mn-doped powders potentially allows for the observed differences in the *g*-values *vs.* available data for the relevant single crystal or microcrystalline environments [11a,b,17]. In this regard, the EPR measurements would benefit much from smaller manganese concentrations and fine splitting that would provide an additional tool for precise structural referencing. However, this is contrary to what we aimed to achieve in this study, namely, checking the largest possible manganese contents in GaN available *via* the AAVS routes. Some important aspects of manganese incorporation into the GaN matrix can further be addressed by measurements of sample magnetization with temperature and field strength. Such studies are underway and the results will be published elsewhere.

4. Conclusions

In this report, we describe the utilization of the aerosol-assisted vapor phase synthesis method for the preparation of nanocrystalline GaN powders with incorporated manganese centers based on modifications of this versatile method previously applied to make a range of pure BN and GaN powders. Especially, we show that, in addition to aqueous solutions of the commercially available gallium and manganese precursors, we can utilize methanol solutions with definite advantages related to the characteristics of the pure, *e.g.*, GaN, and composite products (less residual oxygen, different morphology, higher concentrations of paramagnetic defects in systems containing manganese).

The product powders from both solution systems are composed of the major h-GaN phase and the minor MnO phase. However, the EPR measurements and preliminary magnetization data support a degree of manganese incorporation into the bulk/surface structure of the h-GaN matrix. In this regard, the data suggest a solution-route-specific Mn-saturation effect with the surplus of manganese resisting nitridation under applied conditions and persisting as MnO in the composites. It is worth to note that the latter component can be removed from the composites by acid washings leading to Mn-doped h-GaN nanopowders.

Acknowledgement

This work was supported by Polish Committee for Scientific Research KBN/AGH University of Science and Technology grant No. 11.11.210.62.

References

[1] H. Morkoç, Potential applications of III–V nitride semiconductors, Mater. Sci. Engng B43 (1997) 137–146. and references therein.

[2] S.J. Pearton, C.R. Abernathy, D.P. Norton, A.F. Hebard, Y.D. Park, L.A. Boatner, J.D. Budai, Advances in wide bandgap materials for semiconductor spintronics, Mater. Sci. Engng R40 (2003) 137–168.

[3] V.G. Golubev, D.A. Kurdyukov, A.V. Medvedev, A.B. Pevtsov, L.M. Sorokin, J.L. Hutchison, Structural and photonic properties of opal–GaN nanocomposites, Semiconductor 35 (2001) 1320–1323.

[4] (a) T.T. Borek, W. Ackerman, D.W. Hua, R.T. Paine, D.M. Smith, Highly microporous boron nitride for gas adsorption, Langmuir 7 (1991) 2844–2846. (b) J.F. Janik, W.C. Ackerman, R.T. Paine, D.W Hua, A. Maskara, D.M. Smith, Boron nitride as a selective gas adsorbent, Langmuir 10 (1994) 514–518.

[5] Q.L. Liu, F.F. Xu, T. Tanaka, Visible emission from N-rich turbostratic boron nitride thin films doped with Eu, Tb, and Tm, Appl. Phys. Lett. 81 (2002) 3948–3950.

[6] X. Li, C. Shao, S. Qiu, F.-S. Xiao, W. Zheng, P. Ying, O. Terasaki, Light-emitting boron nitride nanoparticles encapsulated in zeolite ZSM-5, Microporous Mesoporous Mater. 40 (2000) 263–269.

[7] M. Palczewska, A. Wolos, M. Kaminska, I. Grzegory, M. Bockowski, S. Krukowski, T. Suski, S. Porowski, Electron spin resonance of erbium in gallium nitride, Solid State Commun. 114 (2000) 39–42.

[8] A.J. Steckl, J. Heikenfeld, D.S. Lee, M. Garter, Multiple color capability from rare earth-doped gallium nitride, Mater. Sci. Engng B81 (2001) 97–101.

[9] M. Rubinstein, A. Hanbicki, P. Lubitz, M. Osofsky, J.J. Krebs, B. Jonker, Ferromagnetic resonance in (Ga, Mn)As, J. Magn. Magn. Mater. 250 (2002) 164–169.

[10] (a) F. Zhang, N.F. Chen, X. Liu, Z. Liu, S. Yang, C. Chai, (Ga,Mn,N) compounds growth with mass-analyzed low energy dual ion beam deposition, J. Cryst. Growth 252 (2003) 202–207. (b) H. Hori, S. Sonoda, T. Sasaki, Y. Yamamoto, S. Shimizu, K.-I. Suga, K. Kindo, High-T_c ferromagnetism in diluted magnetic semiconducting GaN:Mn films, Physica B 324 (2002) 142–150.

[11] (a) M. Zając, R. Doradziński, J. Gosk, J. Szczytko, M. Lefeld-Sosnowska, M. Kamińska, A. Twardowski, M. Palczewska, E. Grzanka, W. Głębicki, Magnetic and optical properties of GaMnN magnetic semiconductor, Appl. Phys. Lett. 78 (2001) 1276–1278. (b) M. Zając, J. Gosk, M. Kamińska, A. Twardowski, T. Szyszko, S. Podsiadło, Paramagnetism and antiferromagnetic d–d coupling in GaMnN magnetic semiconductor, Appl. Phys. Lett. 79 (2001) 2432–2434. (c) T. Szyszko, G. Kamler, B. Strojek, G. Weisbrod, S. Podsiadło, L. Adamowicz, W. Gębicki, J. Szczytko, A. Twardowski, K. Sikorski, Growth of bulk $Ga_{1-x}Mn_xN$ single crystals, J. Cryst. Growth 233 (2001) 631–638. (d) R. Dwiliński, R. Doradziński, J. Garczyński, L. Sierzputowski, J.M. Baranowski, M. Kamińska, AMMono method of GaN and AlN production, Diamond Relat. Mater. 7 (1998) 1348–1350.

[12] (a) E.A. Pruss, G.L. Wood, W.J. Kroenke, R.T. Paine, Aerosol assisted vapor synthesis of spherical boron nitride powders, Chem. Mater. 12 (2000) 19–21. (b) G.L. Wood, E.A. Pruss, R.T. Paine, Aerosol-assisted vapor phase synthesis of gallium nitride powder, Chem. Mater. 13 (2001) 12–14.

[13] R.T. Paine, W.J. Kronke, J.F. Janik, G.L. Wood, Nonaqueous borate route to boron nitride powders, US patent prosecution-application number 10/280,456, October 24, 2002.

[14] R. Niewa, Nitridocompounds of manganese: manganese nitrides and nitridomanganates, Z. Kristallogr. 217 (2002) 8–23.

[15] S. Strite, M.E. Lin, H. Morkoç, Progress and prospects for GaN and the III–V nitride semiconductors, Thin Solid Films 231 (1993) 197–210.

[16] (a) W.Q. Han, A. Zettl, Pyrolysis approach to the synthesis of gallium nitride nanorods, Appl. Phys. Lett. 80 (2002) 303–305. (b) S.H. Lee, K.S. Nahm, K.C. Kim, S.H. Ahn, E.K. Suh, M.H. Hong, Growth and TEM characterization of GaN microcrystals using a Ni catalyst, J. Korean Phys. Soc. 41 (2002) 155–159.

[17] P.G. Baranov, Identification of manganese trace impurity in GaN crystals by electron paramagnetic resonance, Semicond. Sci. Technol. 11 (1996) 1843–1846.

[18] X. Lu, C. Chen, S. Husuriano, M.D. Koretsky, Effect of chlorine on the photoluminescence of ZnS:Mn thin films, J. Appl. Phys. 85 (1999) 4154–4159.